JOURNAL OF PROPULSION AND POWER
Vol. 15, No. 3, May–June 1999

Launch Vehicle Dynamic and Control Effects from Solid Rocket Motor Slag Ejection

K. W. Dotson,* J. W. Murdock,† and D. K. Kamimoto‡
The Aerospace Corporation, Los Angeles, California 90009-2957

The effects of the ejection of slag from a Titan IV solid rocket motor upgrade (SRMU) are analyzed at maximum dynamic pressure. It is assumed that the 2500 lb of slag onboard at that time is ejected, and the corresponding thrust perturbation is determined using existing theory for the discharge of an inert body. The event is a hypothetical, critical flight condition not observed during any of the first three launches of the Titan IV with SRMUs. Slag ejection causes sharp thrust transients during blockage of the nozzle throat and blowdown of the motor internal pressure. Control simulations indicate a worst-case SRMU gimbal angle change of 0.51 deg during the event, and small-amplitude limit cycles after the excitation. An aeroelastic analysis yields yaw shear loads and bending moments as high as 13,600 lbf and 5.1 $\times 10^6$ lbf in., respectively, at the aft end of the vehicle. It is shown that the degree of the nozzle throat blockage primarily defines the lateral load magnitudes. The Titan IV has adequate structural and control margins, and the ejection of slag is not a concern for its missions.

Nomenclature

A^* = nominal throat area, in.^{2}
C = aerodynamic force coefficient, dimensionless
$[C^*]$ = system modal damping matrix, lbf s/in. and lbf s/rad
$[C']$ = system diagonal matrix of partial derivatives of C with respect to angle of attack, rad^{-1}
C_f = $T/(pA^*)$, nozzle thrust coefficient, dimensionless
c^* = motor characteristic velocity, in./s
$\{\boldsymbol{f}(t)\}$ = vector of system external forces, lbf
$[I]$ = system modal mass matrix (identity matrix), slugs
$\{\boldsymbol{I}\}$ = identity vector, dimensionless
$[LTMD]$ = transformation matrix for displacement-based loads; e.g., lbf/in. and lbf in./in.
$\{\boldsymbol{l}(t)\}$ = vector of internal loads, lbf and lbf in.
$[N]$ = system aerodynamic stiffness matrix, lbf/rad
$[\dot{N}]$ = system aerodynamic damping matrix, lbf s/in.
n = empirical burn rate exponent, dimensionless
p = instantaneous motor chamber pressure, lbf/in.^{2}
$p_{\max}$ = peak chamber pressure caused by blockage, lbf/in.^{2}
p_0 = nominal motor pressure, lbf/in.^{2}
Q = dynamic pressure, lbf/in.^{2}
$\{\boldsymbol{q}(t)\}$ = vector of system generalized translations and rotations, in. and rad
$\{\dot{\boldsymbol{q}}(t)\}$ = vector of system generalized translational and rotational velocities, in./s and rad/s
$\{\ddot{\boldsymbol{q}}(t)\}$ = vector of system generalized translational and rotational accelerations, in./s^2 and rad/s^2
R = gas constant of the propellant gas, in.^{2}/(s^2 °R)
S = reference area, in.^{2}
T = instantaneous thrust, lbf
T_s = stagnation temperature, °R
T_0 = nominal thrust, lbf
t = time, s
t_0 = time blockage clears throat, s
U = relative wind velocity, in./s
u = flow velocity, in./s
V = free volume in the motor, in.^{3}
$\{\boldsymbol{x}(t)\}$ = vector of physical system translations and rotations, in. and rad
$\dot{y}(t)$ = velocity in direction of y axis, in./s
α = ratio of flow area to throat area, dimensionless
β = angle of attack in yaw plane (also called side slip), rad or deg
$\{\Gamma\}$ = aerodynamic force vector, lbf/rad
θ = rotation, rad
ρ = density of two-phase slag, lbm/in.^{3}
υ = motor characteristic time, s
$[\chi]$ = system modes matrix, dimensionless
$[\omega^2]$ = system modal stiffness matrix, lbf/in. and lbf/rad

Subscripts

a = aerodynamic
c = control (including thrust perturbation)
f = force application points
j = node number
r = rotational motion
s = subset
T = total
t = translational motion
y = y axis; also, yaw plane
z = z axis

Introduction

SLAG collects in solid rocket motors that have submerged nozzles and burn aluminized propellants.[1] The amount of slag that accumulates in the nozzle increases after ignition, and can be substantial prior to burnout for large solid rocket motors, such as the Space Shuttle redesigned solid rocket motor (RSRM),[2] the Titan IV solid rocket motor upgrade (SRMU),[3] and the Ariane 5 Moteur a Propergol Solide (MPS).[4] The latter two are new motors. The SRMU internal geometry and maximum slag pool at the maximum dynamic pressure time are shown in Fig. 1.

Historical Summary

The Space Shuttle has experienced the ejection of slag during several flights. The largest of these events occurred during the 65–80-s time period.[5] The Titan IV with SRMUs, shown in Fig. 2, has

Presented as Paper 98-2009 at the AIAA/ASME/ASCE/AHS/ASC 39th Structures, Structural Dynamics, and Materials Conference, Long Beach, CA, April 20–23, 1998; received May 9, 1998; revision received Sept. 30, 1998; accepted for publication Oct. 8, 1998.

*Engineering Specialist, Structural Dynamics Department, P.O. Box 92957-M4/909. E-mail: kirk.w.dotson@aero.org. Senior Member AIAA.
†Senior Engineering Specialist, Fluid Mechanics Department, P.O. Box 92957-M4/964. Associate Fellow AIAA.
‡Manager, Guidance Analysis Department, P.O. Box 92957-M4/975.

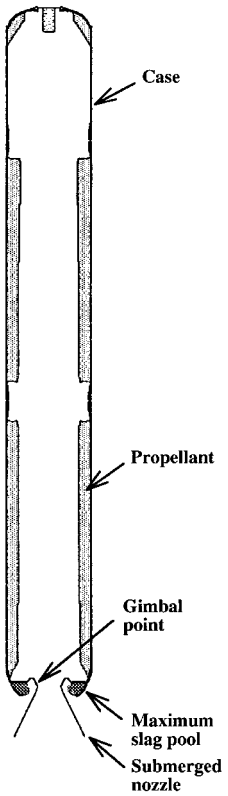

Fig. 1 SRMU internal geometry at maximum dynamic pressure time.

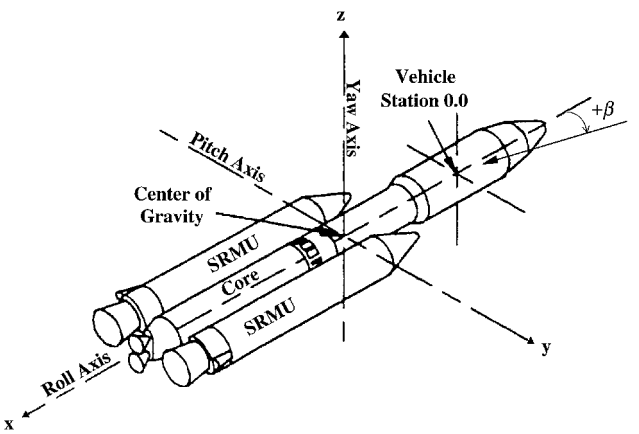

Fig. 2 Titan IV coordinate system for launch vehicle stations and aerodynamic loading.

flown three times. Flight data for these missions did not indicate an ejection of slag during the SRMU burn. The first successful Ariane 5 was launched in 1997; no MPS anomalies were reported.[6]

Several mechanisms for the ejection of slag have been postulated for the Space Shuttle: it has been demonstrated during RSRM (horizontal) ground tests that nozzle vectoring induces slag ejection[2]; flight data indicate that sloshing of the molten slag induces slag expulsion[5]; computational fluid dynamics show that flow field changes caused by the growth of the slag pool can alone cause an ejection[7]; and finally, it has been theorized,[8] based on cold-flow studies,[9] that vortical flow in the aft dome can periodically flush slag from the submerged nozzle. Each of these scenarios can occur even if the slag pool is not close to the lip of the submerged nozzle. Slag ejection occurred during at least one (vertical) static firing test of the SRMU, and real-time radiography corroborates the RSRM conclusion that slag can be ejected during nozzle vectoring.[10]

Impact on Launch Vehicle Loads and Controls

During a slag ejection event, the motor chamber pressure increases, producing a longitudinal thrust perturbation. For the Titan IV, Space Shuttle, and Ariane 5 launch vehicles, maximum dynamic pressure is reached ~56, 66, and 68 s after liftoff, respectively.[11] Because the submerged nozzle does not have to be full for slag to be ejected, and because significant events may occur during the period of maximum airloading, slag ejection can affect the total airloads that launch vehicles with large solid rocket motors must withstand. Along with the liftoff event, maximum airloading induces the most important loads for the design of launch vehicles.[12]

Loads on the Space Shuttle external tank were computed during investigations of RSRM pressure perturbations[13]; it was assumed in these analyses that the vehicle is trim at every instant of time during the event and that the vehicle response is quasistatic.[14] The objective of this work is to formulate a more rigorous analysis of the dynamic response of a launch vehicle induced by slag ejection, and to evaluate the impact on load and stability margins. The problem is challenging because it involves fluid mechanics, aeroelasticity, and control-structure interaction. Numerous studies have addressed spacecraft coning instabilities caused by slag sloshing,[15–17] but the dynamic and control effects from slag ejection do not appear to have been investigated.

Predictions are presented herein for the Titan IV mission with the Cassini spacecraft launched in October 1997. The slag ejection event is assumed to occur at the time of maximum dynamic pressure. Slag continues to accumulate after maximum airloading such that the slag pool surface is closer to the nozzle lip at later times.[3] The likelihood of a large amount of slag being ejected is, therefore, higher at the end of the motor burn than during airloading and must be accounted for in the analysis of solid rocket motor separation from the vehicle core. Such an event, however, is generally not a load concern, but affects the clearance between the solid rocket motors and other components. Clearance loss caused by slag ejection during solid rocket motor separation has been assessed[18] for the Titan IV, but it is beyond the scope of this paper.

Analysis Approach

To analyze the problem, it is necessary to consider the slag-ejection event separately from buffeting, maneuvering, or wind gusts, which also occur during maximum airloading,[19] even though one of these events may actually trigger the ejection. This approach is used for the calculation of maximum airloads because it is impossible to predict the exact amplitude, frequency content, and time phasing of these events prior to flight.[19] Results from the slag-ejection analysis are ultimately incorporated with the other constituent airloads, using a combination equation[20] to define its impact on the total airloads.

It is further assumed that slag is ejected from only one solid rocket motor, namely, the SRMU on the negative side of the y axis in Fig. 2. This scenario produces the highest external yaw moment. Space Shuttle experience corroborates this assumption because the ejection of slag from both motors simultaneously was not observed.[13]

The thrust forcing function corresponding to the slag ejection is established by solving the differential equations for inert mass ejection using techniques developed in Ref. 21. This is accomplished by analyzing independently 1) the blockage of the nozzle throat by the slag and 2) the blowdown of the motor after the throat blockage is removed. The signature of the thrust perturbation is a function of the mass of the slag ejected. The value chosen for the Titan IV load analysis is consistent with statistical estimates based on measurements of slag accumulation during, and after, the five SRMU static firing tests.[22]

Flight simulations with the predicted thrust time history are next conducted to establish the response of the control system during the slag ejection event. The outputs of this analysis are time histories of the angle of attack and SRMU side force, which represent the launch vehicle responding to the sudden change in the longitudinal thrust and steering to eliminate the imposed angular acceleration. In addition, vehicle controllability is assessed through computation of limit cycle amplitudes for the nonlinear control system. It is shown that the ejection of slag has a negligible effect on the vehicle control capability for the Titan IV.

The thrust time history and the outputs from the flight-control analysis are finally used in a load analysis of the launch vehicle. The results show that a slag ejection event can generate significant yaw shear loads and bending moments, particularly at the aft end of the launch vehicle. It is, therefore, concluded that slag ejection should be considered as a load event for launch vehicles that have low structural margins in this vicinity. These loads may also, in this case, affect day-of-launch assessments of the flight winds that the vehicle can withstand.[20] The Titan IV has adequate structural margin, and slag ejection does not reduce its launch availability.

Prediction of Thrust Perturbation

Available RSRM data,[1,2,13] in conjunction with a previous study[21] on inert mass ejection, are used to produce conservative estimates of the pressure and thrust perturbations that can be expected for the Titan IV SRMU.

Space Shuttle RSRM

NASA has surveyed all of their flight data and found that the largest slag ejection event occurred on mission STS-54.[13] One motor on this flight exhibited a chamber pressure perturbation of 13 psi at 67 s into the burn. Using these data, it was concluded[13] that the 13-psi perturbation could have been caused by a nozzle throat blockage of 47.5 in.^{2} acting for 0.8 s. However, a subsequent calculation[1] found that a 45-in.^{2} blockage acting for 0.8 s resulted in a 16-psi perturbation. In addition, a vehicle thrust imbalance of 76,000 lbf was present at the time of this event. NASA states, however, that only a thrust imbalance of 51,000 lbf is associated with the 13-psi pressure perturbation; the remaining 25,000 lbf is a bias that existed before the slag ejection event. Finally, it is stated[13] that the statistical variation of the data indicate a 20-psi perturbation with 2400 lb of slag ejected is the maximum possible event.

To understand and to scale these data, a model is constructed for the 20-psi, worst-case event. The model facilitates self-consistency tests of the data and shows where these data fit relative to previous inert mass ejection calculations.[21] This model is a perturbation caused by slag ejection only about a nominal, constant state.

Consider the quasisteady pressure increase inside a solid rocket motor caused by slag exiting the nozzle and partially blocking the throat. The governing equation, neglecting any time rate of change of burning area, is

$$\frac{\mathrm{d}(p/p_0)}{\mathrm{d}(t/\upsilon)} = \left(\frac{p}{p_0}\right)^n - \frac{\alpha p}{p_0} \tag{1}$$

This equation comes from conservation of mass; the left side is proportional to the time rate of change of mass in the motor. The terms on the right represent the mass flux from the burning surface and the throat mass flow, respectively.

The characteristic time of the motor is defined as

$$\upsilon = \frac{c^* V}{R T_s A^*} \tag{2}$$

The physical interpretation of υ is the time to exhaust the gas contained in the motor free volume through the nozzle throat. If the throat blockage is introduced at time zero and α is constant thereafter, Eq. (1) can be integrated analytically such that

$$\frac{p}{p_0} = \left\{\frac{1-(1-\alpha)\exp[-\alpha(1-n)t/\upsilon]}{\alpha}\right\}^{1/(1-n)} \tag{3}$$

The use of a dimensionless flow area α that is discontinuous in time is an approximation that allows Eq. (1) to be integrated analytically and, thereby, elucidates the physics of slag ejection. Equation (1) is a first order ordinary differential equation that could be integrated numerically for continuous $\alpha(t)$. As will be shown, the constant α approximation produces a conservative approximation to the thrust. Because this thrust does not cause a problem for the Titan IV vehicle, the model is not refined further.

An equation similar to Eq. (1) applies for the blowdown of the motor after the slag-induced throat blockage is removed, and α returns to unity:

$$\frac{\mathrm{d}(p/p_0)}{\mathrm{d}(t/\upsilon)} = \left(\frac{p}{p_0}\right)^n - \frac{p}{p_0} \tag{4}$$

The analytical solution of Eq. (4) is

$$\frac{p}{p_0} = \left\{1 + \left[\left(\frac{p_{\max}}{p_0}\right)^{1-n} - 1\right]\exp\left[\frac{-(1-n)(t-t_0)}{\upsilon}\right]\right\}^{1/(1-n)} \qquad 1 > t_0 \tag{5}$$

Consider the motor thrust. Reference 21 shows that, except for brief transients, a quasisteady flow approximation gives a good estimate for the thrust during periods of nozzle blockage. When the throat is blocked, there is a gas contribution and an inert mass contribution to the thrust. For the gas, the nominal thrust coefficient C_f is adequate; when used with the gas flow area, this results in a gas thrust proportional to the unblocked throat area. To this must be added the contribution of the slag mass, which can be approximated by a C_f of unity (where the stagnation pressure times the blocked area equals this portion of the thrust).[21] Thus, it is assumed that, while the blockage is acting, the dimensionless thrust is given by

$$T/T_0 = [\alpha + (1-\alpha)/C_f](p/p_0) \tag{6}$$

and after the blockage has cleared the dimensionless thrust and pressure are equal, i.e.,

$$T/T_0 = p/p_0 \tag{7}$$

At 67 s into the RSRM burn, $\upsilon = 0.272$ s and $p_0 = 635$ psi. The 0.8-s throat blockage required to produce a 20-psi pressure rise may be found by substituting these values and $n = 0.35$ into Eq. (3). The quantity α is found to be 0.9765, corresponding to a 57.6-in.^{2} physical blockage. With α and C_f (=1.67) known, the dimensionless pressure and thrust can be computed as functions of time using the preceding equations. The results are shown in Fig. 3, along with the dimensionless throat area that is the underlying cause.

Note that the pressure rises continuously from unity to its peak and then decays back to the nominal value. The thrust, however, drops discontinuously when the blockage enters the throat, rises continuously to above unity, rises discontinuously when the blockage clears, and then finally decays continuously to unity. The behavior of the thrust is a direct result of the discontinuous blockage assumed herein. The discontinuous thrust exacerbates the vehicle dynamic response, which makes this approximation conservative. The behavior in Fig. 3 is very similar to that found in an earlier, fully transient study[21] of inert mass discharge, lending confidence in the present approach.

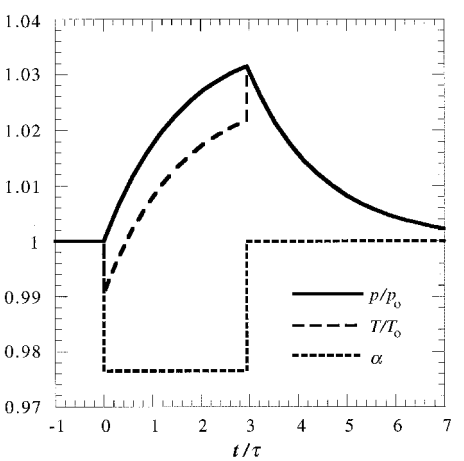

Fig. 3 RSRM dimensionless pressure, thrust, and flow area.

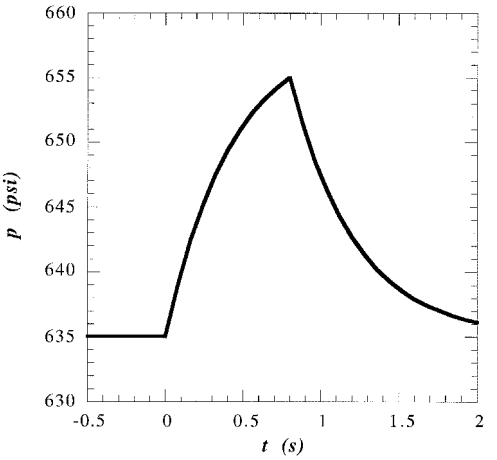

Fig. 4 RSRM pressure.

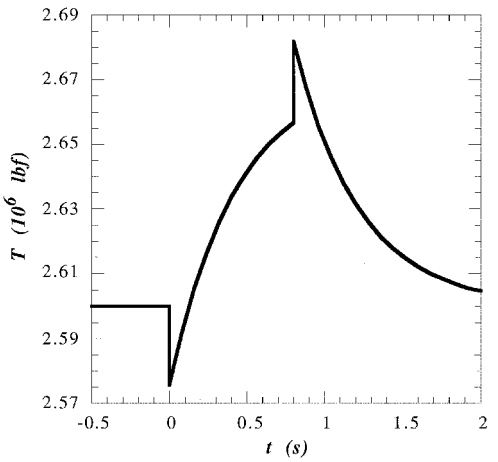

Fig. 5 RSRM thrust.

Some gross, self-consistency checks are possible. The NASA worst case used herein states that 2400 lb of slag can cause the 20-psi rise shown in Fig. 4. The present calculations show that this requires a 0.8-s, 57.6-in.^{2} throat blockage. Conservation of mass requires a mass velocity ρu of 52.1 lbm/s in.^{2} for the slag passing through the throat. We note that only the product ρu is defined by this calculation; the density ρ is unknown because it is most likely a mixture of liquid aluminum oxide and evolving gases. The upper bound for ρ is the single-phase 0.069-lbm/in.^{3} value. Using this liquid density shows that the slag or the two-phase mixture is flowing through the throat at an average velocity equal to or greater than 750 in./s. This quantity is physically reasonable for two reasons. First, if a filament of slag extends from the nozzle entrance to the throat plane, it sees a pressure drop of about half of $p_0 = 635$ psi. The Bernoulli equation for incompressible flow applies if there are continuous liquid streamlines. Using this pressure drop gives a liquid velocity at the throat of 1880 in./s. This velocity implies either a two-phase density 40% of the liquid density, a pure liquid film experiencing significant liquid drag from the nozzle wall, or some intermediate case. A second sanity check shows that the throat velocity of the slag is of the same order as that of the inert solid masses studied in Ref. 21.

The dimensional thrust is of primary interest for the dynamic and control assessments. It is shown, subject to the stated assumptions, in Fig. 5, where $T_0 = 2.6 \times 10^6$ lbf has been used for the RSRM at 67 s into the burn.

Using Fig. 5, two further sanity checks can be made. First, the curve in Fig. 5 is integrated to compute the change in impulse associated with the slag ejection. This impulse is used to define (a fictitious) specific impulse (I_{sp}) associated with the slag, i.e., the impulse change divided by the total ejected slag mass. This operation when applied to Fig. 5 gives an equivalent slag I_{sp} of 23.6 s. This is the same order as the more detailed calculations of Ref. 21, where the inert mass I_{sp} varied between about 9 and 18 s. Finally, it is noted that the NASA worst-case data had a measured peak pressure perturbation of 13 psi and a thrust perturbation of 51,000 lbf. These quantities are in about the same ratio in the present model; the peak pressure and thrust perturbation are 20 psi and 82,000 lbf, respectively. The model is found to be consistent with known data and with prior calculations,[21] and hence, will be scaled to the SRMU in the following section.

Titan IV SRMU

The nominal values of SRMU chamber pressure and thrust are taken to be 879 psi and 1.4×10^6 lbf, respectively, when maximum dynamic pressure occurs. The maximum amount of slag contained in the recessed nozzle equals roughly 2500 lb at the maximum dynamic pressure time.[22] The maximum slag amount increases to 5500 lb at motor burnout.[22] For conservatism, we assume that it is all ejected, although this is deemed very unlikely to occur. The time to dump this slag (as compared with the RSRM) is taken to scale directly with mass and inversely with liquid velocity (square root of pressure), i.e.,

$$t_0 \approx 0.8s\left(\frac{2500\ \text{lbf}}{2400\ \text{lbf}}\right)\left(\frac{635\ \text{psi}}{879\ \text{psi}}\right)^{\frac{1}{2}} = 0.7s \tag{8}$$

Hence, it is assumed that 2500 lb of slag is ejected in 0.7 s. In the case of the RSRM, the maximum-density slag passed through the throat at 40% of the Bernoulli velocity. If that assumption is made here, then by conservation of mass, the blockage area in the throat is 58.2 in.^{2} and α is 0.9394. Using these values with $\upsilon = 0.305$ s and $n = 0.278$, it is possible to compute the thrust and pressure time histories with the given equations. The dimensionless quantities are shown in Fig. 6.

The character of Fig. 6 is very similar to Fig. 3, except for the fact that the magnitudes of the dimensionless perturbations are larger. This is to be expected, however, because the SRMU is a smaller motor ejecting about the same mass of slag as the RSRM.

The SRMU pressure time history is shown in Fig. 7. In this case, the peak perturbation is about 62 psi. This is significantly greater than the 20 psi maximum for the RSRM. The thrust time history is displayed in Fig. 8. The worst-case thrust perturbation equals 99,500 lbf, which is also significantly larger than for the RSRM.

The total impulse perturbation associated with Fig. 8 has also been computed for comparison with the Space Shuttle. Normalizing the impulse with the slag mass, as before, gives an equivalent I_{sp} of 24.2 s, which is comparable to both the RSRM value and the inert mass values.[21]

Parametric Study

The preceding analysis for the Titan IV SRMU, in which 2500 lb of slag is ejected, is believed to represent a worst-case scenario because of the discontinuous nature of the blockage and because the

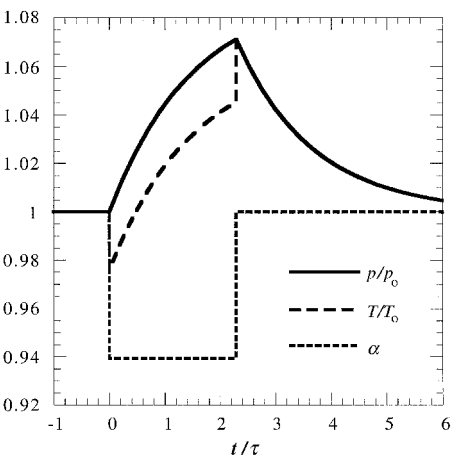

Fig. 6 SRMU dimensionless pressure, thrust, and flow area.

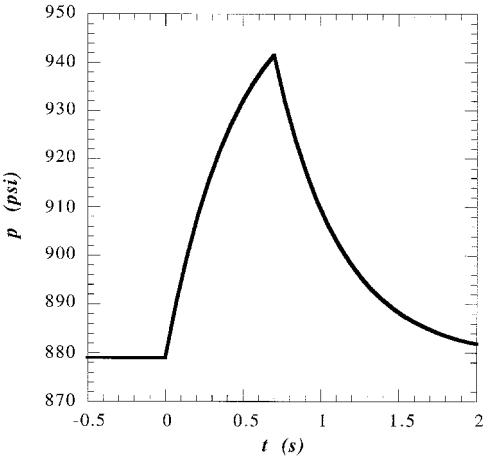

Fig. 7 SRMU pressure.

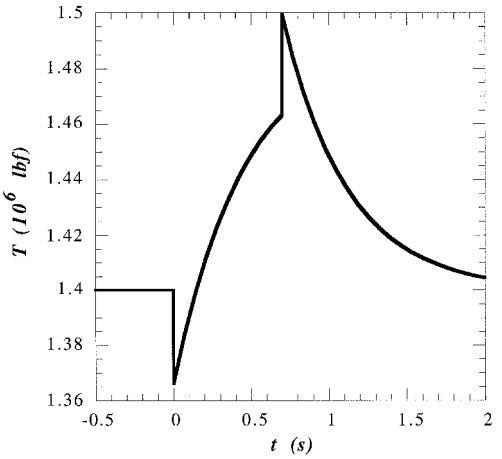

Fig. 8 SRMU thrust.

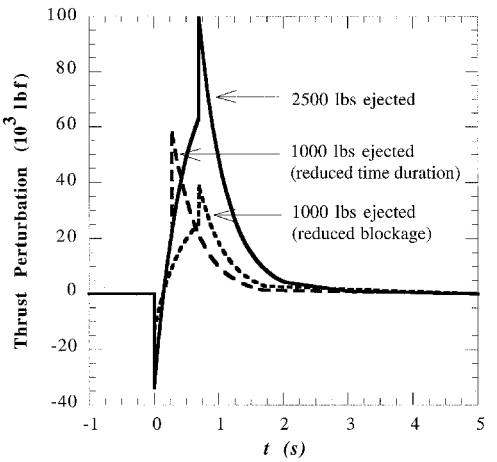

Fig. 9 Thrust perturbations for Titan IV load cases.

total slag mass is ejected. To investigate the effects of the mechanism on the resulting launch vehicle loads, the ejection of 1000 lb of slag was also analyzed. The reduction in slag mass was accounted for in two ways: 1) through a decrease in the nozzle throat blockage and 2) through a decrease in the time duration of the blockage. The resulting thrust perturbation time histories are shown in Fig. 9.

Flight-Control Simulation

A flight-control simulation was conducted to demonstrate the vehicle transient response to the slag ejection event, and to provide SRMU nozzle gimbal angles and vehicle angle-of-attack time histories for the load analyses. The slag ejection event was modeled as a worst-case perturbing moment in the yaw plane created by the asymmetric change in thrust. The simulation included structural bending modes, a digital autopilot, a high-fidelity nonlinear actuator model, and sloshing of the booster liquid propellants and SRMU slag. The tool was developed primarily for the analysis of limit cycles that contribute to the loads on the vehicle and could cause a loss of control authority.

The dominant nonlinearities for the Titan IV vehicle include engine actuator friction and transducer backlash, as well as quantization associated with the digital autopilot. The Titan IV autopilot consists of an attitude feedback loop, two rate feedback loops for first bending mode stabilization, and a lateral acceleration feedback loop for aerodynamic load alleviation. The digital autopilot operates at 25 Hz, except for the lateral acceleration loop that operates at 100 Hz to prevent aliasing. All of the thrust perturbations shown in Fig. 9 have a dominant frequency less than 2 Hz, which is within the typical bandwidth of the Titan IV autopilot.

The simulation for the case in which 2500 lb of slag is ejected is shown in Fig. 10. The maximum SRMU gimbal angle seen during the event equals 0.51 deg. This is well below the limit of 4.5 deg at the maximum dynamic pressure time. After the excitation, small oscillations occur as a result of nonlinearities in the SRMU nozzle actuators and quantization in the signal A/D conversion. The frequency of the oscillations is below 1 Hz and coincides with that for sloshing of the booster liquid propellants and SRMU slag. The amplitudes of these oscillations, however, are well below the limit cycle specification of 0.3 deg. These results show that slag ejection is not a flight-control concern for the Titan IV.

SRMU yaw side force time histories from the control simulation are shown in Fig. 11 for the three Titan IV load cases. Because

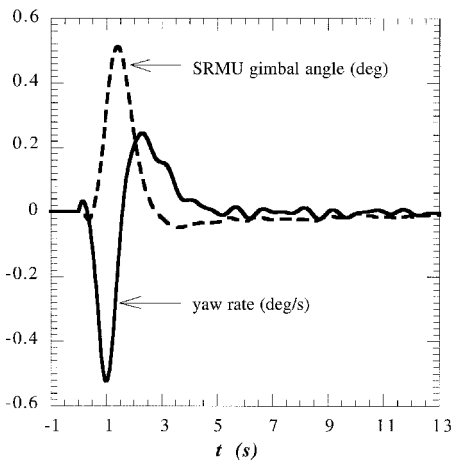

Fig. 10 Titan IV control outputs for 2500-lb slag ejection case.

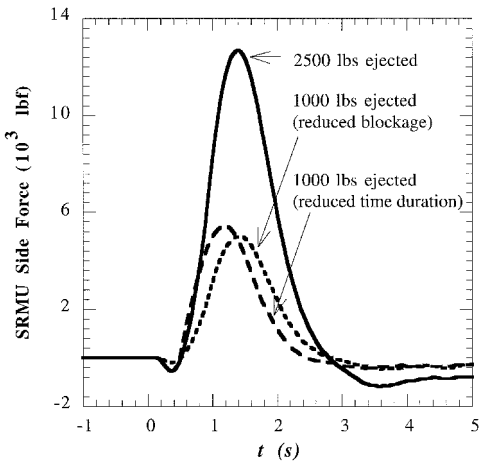

Fig. 11 SRMU yaw side force for Titan IV load cases.

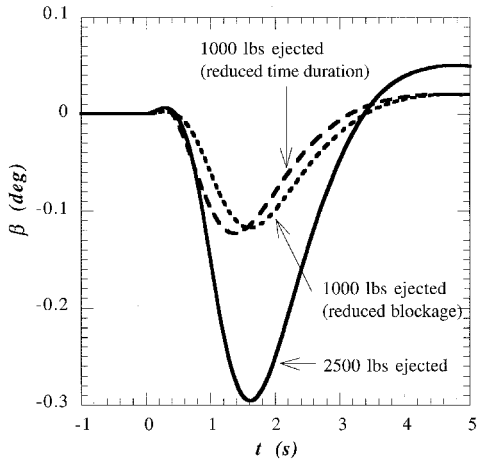

Fig. 12 Yaw plane angle of attack for Titan IV load cases.

the instantaneous gimbal angle is always small (see Fig. 10), these curves were obtained by simply scaling the gimbal angle histories by the instantaneous thrust. The latter is defined as the sum of the nominal thrust (1.4×10^6 lbf) and the thrust perturbation from Fig. 9. The yaw side force acts at the gimbal point, shown in Fig. 1, of each SRMU.

The rigid-body yaw angle-of-attack (side-slip) histories from the control simulations are shown in Fig. 12 for the three load cases. The angle-of-attack histories generate external launch vehicle aerodynamic forces that must be included in the load analysis.

Prediction of Launch Vehicle Loads

The coupled dynamic system is next analyzed open loop using the force and angle-of-attack time histories from the control simulation. The control and load assessments are not integrated into a single analysis because the complexity cannot be justified; viz., a large set of system modes makes the control analysis too cumbersome, and the full control system model is too complex to incorporate in the load analysis. The application of externally defined control forces in an open-loop dynamic analysis was also used in the analysis of launch vehicle loads from maneuvering through measured flight winds.[23]

Aeroelastic Equations of Motion

The modal equations of motion are defined by

$$[I]\{\ddot{q}(t)\} + [C^*]\{\dot{q}(t)\} + [\omega^2]\{q(t)\} = [\chi]_f^T\{f(t)\} \tag{9}$$

in which

$$\{x(t)\} = [\chi]\{q(t)\} \tag{10}$$

The vector $\{f(t)\}$ includes both the aerodynamic and control forces. The modal matrices in Eq. (9) were generated for the Titan IV using the Benfield–Hruda component coupling procedure[24] with subsystem dynamic models. The Titan IV coupled system model was truncated at 20 Hz for the slag ejection load analysis. It was validated that sufficient modes were retained for launch vehicle load convergence.

In the Titan IV coordinate system, at node j of the dynamic model, the aerodynamic forces in the yaw plane are defined by

$$f_{a,j}(t) = QS\left(\frac{\partial C_y}{\partial \beta}\right)_j \beta_{T,j}(t) \tag{11}$$

in which the term in the parentheses represents the change in the dimensionless aerodynamic normal force with angle of attack at node j. The angle of attack at node j, including the local effects, is defined by

$$\beta_{T,j}(t) = \beta(t) - \left[\frac{\dot{y}_j(t)}{U}\right] - \theta_{z,j}(t) \tag{12}$$

Substituting Eq. (12) into Eq. (11), and writing the equations for the model nodes in matrix notation, yields

$$\{f_a(t)\} = QS[C_y']\left(\{I\}\beta(t) - \left\{\frac{\dot{y}(t)}{U}\right\} - \{\theta_z(t)\}\right) \tag{13}$$

Substituting Eq. (13) into Eq. (9) yields

$$[I]\{\ddot{q}(t)\} + ([C^*] + [\dot{N}_y])\{\dot{q}(t)\} + \left([\omega^2] + [N_y]\right)\{q(t)\} = [\chi]_f^T\{f_s(t)\} \tag{14}$$

in which

$$[N_y] = QS[\chi_{ty}]^T[C_y'][\chi_{rz}] \tag{15}$$

$$[\dot{N}_y] = (QS/U)[\chi_{ty}]^T[C_y'][\chi_{ty}] \tag{16}$$

$$[\chi]_f^T\{f_s(t)\} = \{\Gamma_y\}\beta(t) + [\chi]_c^T\{f_c(t)\} \tag{17}$$

in which

$$\{\Gamma_y\} = QS[\chi_{ty}]^T[C_y']\{I\} \tag{18}$$

The local effects of the yaw plane rotation and velocity along the vehicle length are accounted for in the aerodynamic stiffness and damping matrices, respectively. The vector $\{f_s(t)\}$ contains the thrust perturbation, the SRMU side forces, and the aerodynamic forces caused by the rigid-body angle of attack.

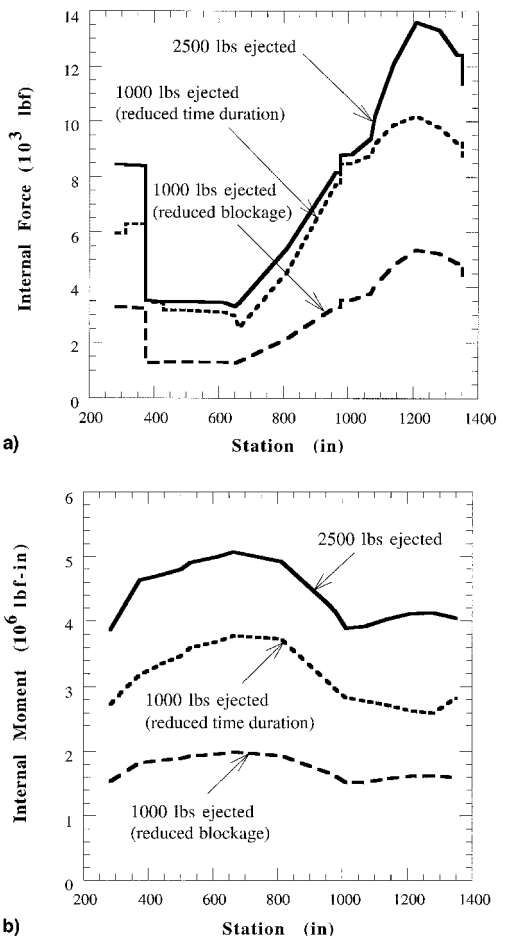

Fig. 13 Predicted Titan IV launch vehicle loads for slag ejection event: a) yaw shear and b) yaw bending moment.

Recovery of Launch Vehicle Loads

A transient response code that uses the coupled system matrices solves Eq. (14) for the time histories $\{\ddot{q}(t)\}$, $\{\dot{q}(t)\}$, and $\{q(t)\}$. Launch vehicle loads are then computed from the transformation

$$\{I(t)\} = [LTMD]\{x(t)\} = [LTMD][\chi]\{q(t)\} \tag{19}$$

The matrix [*LTMD*] is produced from the finite element model for the launch vehicle, and generally corresponds to the six internal loads (three forces and three moments) at each of the vehicle nodes. However, for the slag ejection analysis, the pitch plane loads are negligible because the excitation is solely in the yaw plane.

Results for Mission with Cassini Spacecraft

The absolute maximum values of the internal yaw shear and bending moment are plotted in Fig. 13 as a function of vehicle station for the three load cases. The stations increase in the direction of the x axis, as shown in Fig. 2. Only loads for the aft portion of the vehicle core are plotted; loads forward of these stations diminish to zero.

Figure 13 shows that the salient parameter in the determination of the magnitude of the lateral launch vehicle loads is the degree of the nozzle throat blockage. Decreasing the blockage markedly reduces these loads. Decreasing the duration of the blockage is not as effective. This means that, provided the nozzle throat blockage is constant, the lateral launch vehicle loads may be significant even if only a portion of the slag pool is ejected.

The plotted results also indicate that the worst-case slag ejection loads can be scaled by 1000/2500 to estimate those for 1000 lb of ejected slag (with the reduced nozzle throat blockage). This might have been anticipated because the thrust perturbation (Fig. 9), SRMU side force (Fig. 11), and angle-of-attack (Fig. 12) time histories roughly scale with respect to the slag ejection mass, provided that the nozzle throat blockage is variable.

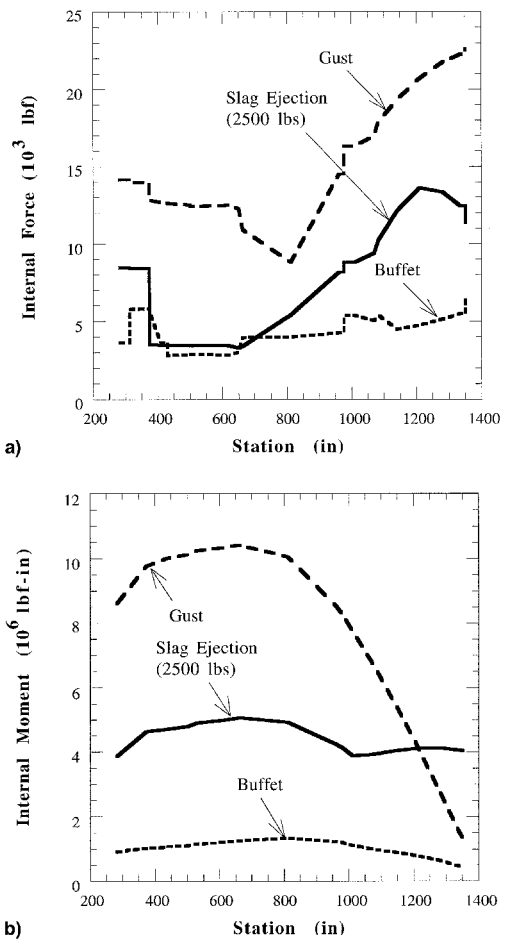

Fig. 14 Comparison of predicted slag ejection, gust, and buffet launch vehicle loads: a) yaw shear and b) yaw bending moment.

The yaw shear loads and bending moments, for the case in which 2500 lb of slag is ejected, are compared in Fig. 14 with prelaunch predictions of gust and buffet loads at the maximum dynamic pressure time. It can be concluded from Fig. 14 that the ejection of slag from solid rocket motors with recessed nozzles induces significant loads that should be combined statistically with those for the other airload contributors.[19,20] The loads are of particular concern at the aft end of the vehicle, where the yaw bending moments induced by slag ejection may even exceed those predicted for the gust event.

Total airloads are computed as the sum of the mean load terms for the flight events and the rss of the corresponding load dispersions.[20,23] In this study, the slag ejection loads were treated strictly as load dispersions because they are not believed to possess a mean component, as do loads for the buffeting, gust, and maneuvering events. The implication is that slag ejection is rare for the Titan IV. Flight data from the first three launches of the Titan IV with SRMUs corroborate this approach because they indicate that a slag ejection event has yet to occur.

The load combination revealed that a slag ejection event significantly increases the total airloads at the aft end of the Titan IV. However, the total airloads increase only slightly at the middle of the core, where the structural margins are the lowest. At these critical vehicle stations, the values increase about 1% when 2500 lb of slag are ejected. The impact would, of course, be much greater if slag ejection events were common, justifying the use of a mean load component.

Conclusions

The thrust transient during solid rocket motor slag ejection has been analyzed using a model that admits a closed-form solution. Conservative assumptions were used to define the worst-case load and control conditions. Space Shuttle experience with slag ejection was exploited and RSRM data were scaled to the Titan IV SRMU in a physically realistic way.

Using the model, it was found that slag ejection from SRMUs is not a control concern for the Titan IV, but that the induced loads may be substantial, particularly at the aft end of the vehicle. The Titan IV, however, has adequate structural margin. The degree of the nozzle throat blockage, instead of the ejected slag mass, primarily establishes the Titan IV lateral load magnitudes. This may be the case for other large launch vehicles with solid rocket motors as stages, and suggests that the induced loads may be significant even when the volume of accumulated slag is not large.

References

[1]Salita, M., "Deficiencies and Requirements in Modeling of Slag Generation in Solid Rocket Motors," *Journal of Propulsion and Power*, Vol. 11, No. 1, 1995, pp. 10–23.

[2]Sambamurthi, J. K., Alvarado, A., and Mathias, E. C., "Correlation of Slag Expulsion with Ballistic Anomalies in Shuttle Solid Rocket Motors," *Journal of Propulsion and Power*, Vol. 12, No. 4, 1996, pp. 625–631.

[3]Johnston, W. A., Murdock, J. W., Koshigoe, S., and Than, P. T., "Slag Accumulation in the Titan Solid Rocket Motor Upgrade," *Journal of Propulsion and Power*, Vol. 11, No. 5, 1995, pp. 1012–1020.

[4]Chauvot, J.-F., Dumas, L., and Schmeisser, K., "Modeling of Alumina Slag Formation in Solid Rocket Motors," AIAA Paper 95-2729, July 1995.

[5]Hopson, C., "Space Shuttle Solid Rocket Motor Slag Expulsion Mechanisms," AIAA Paper 95-2725, July 1995.

[6]Sparaco, P., "Ariane 5 Succeeds on Its Second Try," *Aviation Week & Space Technology*, Nov. 3, 1997, pp. 22, 23.

[7]Liaw, P., Chen, Y.-S., Shang, H.-M., and Doran, D., "Numerical Investigation of the Slag Behavior in the Aft-End Cavity of Solid Rocket Motors," AIAA Paper 95-21773, Jan. 1995.

[8]Whitesides, R. H., Purinton, D. C., Hengel, J. E., and Skelley, S. E., "Effects of Slag Ejection on Solid Rocket Motor Performance," AIAA Paper 95-2724, July 1995.

[9]Waesche, R. H. W., Sargent, W. H., and Marchman, J. F., III, "Space Shuttle Solid Rocket Motor Aft-End Internal Flows," *Journal of Propulsion and Power*, Vol. 5, No. 6, 1989, pp. 650–656.

[10]Dolan, K. W., Curnow, G. M., Perkins, D. E., Costerus, B. W., La Chapell, M. J., Turner, D. E., Wallace, P. W., and Schneberk, D. E., "Real-Time Radiography of Titan IV SRMU Static Firing Test QM2," Lawrence Livermore National Lab., UCRL-CR-117148, Livermore, CA, May 1993.

[11] Isakowitz, S. J., *International Reference Guide to Space Launch Systems*, 2nd ed., AIAA, Washington, DC, 1995, pp. 44, 287.

[12] Fleming, E. R., "Launch Vehicle Loads," *Flight-Vehicle Materials, Structures, and Dynamics—Assessment and Future Directions. Vol. 1—New and Projected Aeronautical and Space Systems, Design Concepts, and Loads*, Sec. 2, A95-24426, The American Society of Mechanical Engineers, New York, 1994, pp. 530–541.

[13] Altman, D., Culick, F., Faget, M. A., Price, E. W., Summerfield, M., and Thibodaux, G., "Report of Special Investigating Committee on Space Shuttle Solid Rocket Motor Pressure Perturbations," NASA, Washington, DC, Jan. 1994.

[14] Structural Loads Group, "Structural Design Loads Data Book," Boeing North American, NASA STS 85-0169, Downey, CA, Sept. 1997.

[15] Yam, Y., Mingori, D. L., and Halsmer, D. M., "Stability of a Spinning Axisymmetric Rocket with Dissipative Internal Mass Motion," *Journal of Guidance, Control, and Dynamics*, Vol. 20, No. 2, 1997, pp. 306–312.

[16] Meyer, R. X., "Coning Instability of Spacecraft During Periods of Thrust," *Journal of Spacecraft and Rockets*, Vol. 33, No. 6, 1996, pp. 781–788.

[17] Or, A. C., and Challoner, A. D., "Stability of Spinning Spacecraft Containing Shallow Pool of Liquid Under Thrust," *Journal of Guidance, Control, and Dynamics*, Vol. 17, No. 5, 1994, pp. 1019–1027.

[18] Au-Yeung, V., "Titan IV/Type II Step 0/Stage I Separation Analysis," Lockheed Martin Astronautics, MCR-93-2587, Denver, CO, Jan. 1994.

[19] Kabe, A. M., "Design and Verification of Launch and Space Vehicle Structures," AIAA Paper 98-1718, April 1998.

[20] Macheske, V. M., Womack, J. M., and Binkley, J. F., "A Statistical Technique for Combining Launch Vehicle Loads During Atmospheric Flight," AIAA Paper 93-0755, Jan. 1993.

[21] Murdock, J. W., "Rocket Thrust Perturbation from Discharge of an Inert Body," *Journal of Propulsion and Power*, Vol. 2, No. 2, 1986, pp. 117–123.

[22] Bruce, J. R., "Slag Slosh Methodology," Lockheed Martin Astronautics, IOM 3323/CB-94-236, Denver, CO, Aug. 1994.

[23] Dotson, K. W., and Tiwari, S. B., "Formulation and Analysis of Launch Vehicle Maneuvering Loads," *Journal of Spacecraft and Rockets*, Vol. 33, No. 6, 1996, pp. 815–821.

[24] Benfield, W. A., and Hruda, R. F., "Vibration Analysis of Structures by Component Mode Substitution," *AIAA Journal*, Vol. 9, No. 7, 1971, pp. 1255–1261.